The concept of rod-driven locomotion for spherical lunar exploration robots

Jasper Zevering*, Dorit Borrmann, Anton Bredenbeck, Andreas Nüchter[1]

***Abstract*— A spherical robotic probe has several advantages in rough environments and has therefore raised interest for application in planetary exploration. A sphere is well-suited to protect high-sensitive payloads, however, the locomotion system for planetary surfaces raises several challenges. This paper presents a novel locomotion system consisting of linear actuators which are usable in a multi-functional fashion. Apart from pushing and bringing leverage for locomotion the extendable rods enable a tripod mode for improved sensing. The developed solutions offer a mathematical-physical system description, simple algorithms for the control of locomotion and balancing as well as general calculations for determining the maximum achievable performance parameters of such a robot. The first built prototype shows the basic suitability of the system and reveals directions for further research.**

INTRODUCTION

The European Space Agency (ESA) has reached out for robotic solutions for exploring and mapping lava caves and tubes on the Moon via an Open Space Innovation Platform system study. The largely unknown environment of lunar caves is challenging and poses great risks to the robot and especially to its sensors. However, some aspects of the cave environment are already known, such as the presence of very sharp rocks due to lack of erosion by wind. This is adverse to most robotic designs currently used in space exploration. As a novel approach, a spherical robot design has been presented within the DAEDALUS project [1]. The spherical shell of the robot protects the sensors such as laser scanners, optical sensors and dosimeters from the harsh conditions. Unlike wheeled robots, which are usually designed for specific environments, a sphere works in a wide range of possible terrains. A sphere with shock-resistant components safely maneuvers rough terrain, which poses a risk of falling from rocks or cliffs and getting stuck. The mission formulated by ESA was to descend into the lunar pit and explore the caves after reaching the bottom. An external crane performs the descent. Figure 1 shows the DAEDALUS sphere.

Multiple locomotion approaches for spherical robots have already been investigated. Most of them use an internal mechanism, like a weight-shifting pendulum drive or they generate internal momentum which is then compensated by the rotation of the robot. These mainly limit the capabilities of the robot in terms of overcoming obstacles and the suitability for uneven terrain. Therefore we introduce a novel rotation-based locomotion approach, driven by linear actuators. These actuators are versatile, as they are responsible not only for locomotion, but also for overcoming obstacles and initializing tripod mode, which provides a stable capturing pose for images and laser scans, both shown in Figure 1.

RELATED WORK

The vast majority of spherical robots use pendulum drives [6]–[15], weight shifting approaches [16]–[19] or internal drive units (IDUs) [20]–[29]. Internal generation of momentum is also used in many cases [30]–[33] and sometimes deformation of the robot [34]–[39].

Previous work in the field of spherical robots using linear actuators extrinsic to the shell is limited. In [43] Ocampo-Jimenez and his team investigate and describe the approach of an internal pendulum and additionally using small linear actuators for lifting the sphere a little in case it gets stuck. The performed simulation shows the capability to free the sphere when it is stuck between obstacles up to $\frac{1}{8}$ of the height of the robot in comparison to $\frac{1}{10}$ without the usage

* jasper.zevering@uni-wuerzburg.de

[1] All authors are with Informatics VII : Robotics and Telematics - University of Wuerzburg

We acknowledge funding from the ESA Contract No. 4000130925 /20/NL/GLC for the “DAEDALUS – Descent And Exploration in Deep Autonomy of Lava Underground Structures” Open Space Innovation Platform (OSIP) lunar caves-system study and the Elite Network Bavaria (ENB) for providing funds for the academic program “Satellite Technology”.

Fig. 1. The DAEDALUS sphere. From left to right: First, Daedalus sphere is descended into the pit by a crane. Second, DAEDALUS in scanning mode. Third, Different modes of DAEDALUS. Fourth, DAEDALUS overcoming obstacles by pushing with its rods.

of the actuator. This leaves room for improvement, also the actuators are not integrated into the locomotion itself. Kim et al. in 2010 [40] also introduce a prototype using a linear actuator, named Kisbot. It consists of a sphere divided into three parts: one middle ring and two outer semispheres. The rotatable semispheres are mounted onto the middle part and are actuated, and have a linear extendable part. For locomotion, it has two driving modes. One is the pendulum-driven rotation, using the non-homogeneous mass distribution of the rotatable semispheres. The second mode is the wheeling mode, where both extendable parts are extended, resulting in the overall functioning of the robot like a one-wheel car. Nonetheless, the linear extension is also used for locomotion as it allows the sphere to push itself on top of obstacles. Further, extending these parts leads to an abrupt stop, if extended on the side towards which the robot is rolling. Both driving modes are tested and evaluated but for lifting and stopping, the concept is only described and not implemented. The German company Festo AG & Co. KG created BionicWheelBot, that imitates the so-called flic-flac spider [41] and uses its leg setup for walking and rolling. While rolling the round structure itself consists of six legs of the robot, the other two are used for pushing. While walking only the six legs are used for the walking itself as the two, which push during rolling, cannot be used due to mechanical restrictions. The pushing legs have a joint that enables pushing despite a lateral orientation. This way of pushing for rotation comes very close to pushing with linear actuators. As only one pair of legs is used for pushing, this leads to a varying rotational speed during a full rotation.

REQUIREMENTS FOR LUNAR CAVE EXPLORATION

The mission concept of DAEDALUS foresees descending into the pit followed by ground exploration into the cave. During both stages, light detection and ranging (LiDAR) sensors as well as optical sensors scan and map the environment. A crane on the lunar surface accomplishes the descent. On the ground, the sphere relies on its own locomotion system. The ground locomotion is challenged by obstacles and slopes, both of which are unspecified in terms of size and slope. On the moon, two environment factors significantly shape the environment: The lack of degenerative effects such as wind as well as the direct radiation from the sun. In combination they lead to very sharp edges on rocks and extremely fine dust, so called regolith [2], [3]. Both of which are detrimental to many sensors and actuators, that are commonly used in robots. Hence, the sensors and actuators need to be protected from direct contact with the environment under any circumstances. Among others, damaging scenarios that are to be avoided are: scratching of a lens of an optical system; dust causing friction inside gear boxes and motors.

The large uncertainties associated with the environment inside the cave add additional difficulties to the already hard problem. If the terrain were roughly known, i.e,. maximum obstacle size and/or expected slopes, a conventional rover could be sized for these requirements, using existing options for sealing the sensors. But without those parameters and with the possibility of falling from scarps, the need of overcoming holes or encountering sharp obstacles that cannot be avoided as another path may be no option, a sphere is a more optimal choice [4].

All these requirements pose restrictions on the locomotion system. The possibility of objects with steep edges eliminates many of the commonly used locomotion methods for spherical robots. Therefore, we present a novel system that especially considers uneven, rough and unknown terrain.

ROD-DRIVEN LOCOMOTION

For locomotion, the robot holds two stars of eight extendable rods each. Rotation of the sphere leads to translation as the friction between the ground and the shell of the robot causes it to roll forward rather than slipping in place. Hence, the poles are primarily responsible for the rotation and secondarily for translation. For lunar explorations, all actions will be done in a slow and controlled manner. Therefore we introduce in this paper mainly the static analysis of general limitations and capabilities of spherical robots. In further research we will introduce the dynamics of the system, but this would exceed the scope of this paper and does not have impact on the presented algorithm for the locomotion. Therefore we also neglect the friction aspect between extending rods and ground, which has a tremendous effect on the dynamic evaluation, but is neglectable for the static analysis. There are two main ways to initiate rotation. The most intuitive is the rotation by pushing against the ground. The rods that lay on the opposite side of the desired rolling direction extend and push into the ground and thus generate torque for the sphere, leading to rotation. The second approach of creating torque for the sphere is by leverage. As the poles have a weight, extending them without any contact to the ground provides torque due to the weight. To generate rotation in a specific direction, the overall center of mass of the extended rods needs to be towards the rotation direction. A combination of both methods is also possible. To designate the direction unambigously and to identify individual bars, we will indicate the angle ζ_x of a rod with index x as follows. The angle ζ starts from 0 rad directing downward perpendicular to the ground, which is also the gravitational vector, and increases clockwise until reaching 2π rad from the right side. Using this, we describe the two rotation approaches with respect to specific angles.

a) Pushing Approach:
Two parameters characterize the pushing approach. Figure 2 visualizes all variables. The first parameter β determines the starting angle for the extension. β must be greater than 0 rad as a pole extending at exactly 0 rad will create a straight force instead of a torque, pushing the sphere upwards. β needs to be chosen in such a way that the extension causes only torque and no linear motion. The second parameter α is the angle for stopping the rod extension.

Geometric considerations alone yield restrictions for α. $\alpha < 0.5\pi$ rad has to hold true, as a pole extending between 0.5π rad and 1.5π rad never touches the flat ground, and between 1.5π rad and 2π rad it works against the desired

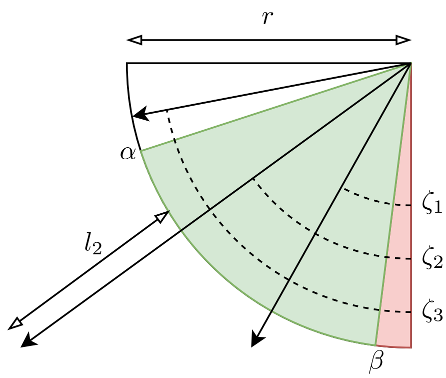

Fig. 2. Variable visualization for the pushing approach. β defines the angle below which a pole does not extend (area marked red), α the angle below which a rod extends (area marked green). ζ_x represents the current angle of rod x. l is the length of a rod, with l_i describing the length of the specific rod with index i. r is the radius of the sphere.

rotation. The maximum extended length of the poles also determines the maximum α. The larger the chosen α, the longer the pole needs to be extended to reach the ground, up to the point where the pole stops pushing despite further extension due to the lack of ground contact. From that moment on, the pole works against the pushing force due to its weight leverage. Assuming that a continuous rotation is desired, the same behavior occurs if the poles cannot vary their extension speed. The steeper the angle to the ground is, the faster the poles need to be extended to cause a constant rotation. This becomes a problem for mono-speed poles.

Let l denote the extension length of a single rod, l_{max} be the maximum possible extension length, and r be the radius of the sphere. Then, α is limited by

$$\alpha \leq \arccos\left(\frac{r}{r + l_{\text{max}}}\right) < \frac{\pi}{2}\,. \tag{1}$$

If the angle ζ_x of a pole is between α and β, then its length l_x must be extended to

$$l_x = \frac{r}{\cos(\zeta_x)} - r\,, \tag{2}$$

in order to touch the flat ground. To obtain the extension speed for a given desired rotational velocity of the sphere, the derivative is formed, leading to

$$\dot{l}_x = \frac{d}{dt}\left(\frac{r}{\cos(\zeta_x)} - r\right) = r \cdot \dot{\zeta}_x \tan(\zeta_x)\sec(\zeta_x)\,, \tag{3}$$

where $\dot{\zeta}_x = \dot{\zeta}_1 = ... = \dot{\zeta}_n$ is the same for all poles and is the rotation speed of the sphere. Figure 3 shows the required extension speed for the rod of a sphere with one meter radius given a desired rotation speed of one rad per second. Consequently, the maximum possible speed of one pole also limits α and/or the maximum possible speed of rotation. By rearranging Equation (3) for $\dot{\zeta}_x$ and substituting the rotation speed of the sphere ω for $\dot{\zeta}_x$ we get

$$\omega = \frac{\dot{l}_x}{r \cdot \tan(\zeta_x)\sec(\zeta_x)}\,. \tag{4}$$

We see that for $\dot{\omega} = 0$ we need a $\dot{l}_x \neq 0, \ddot{l}_x = 0$. This demonstrates the aforementioned inability of poles with only

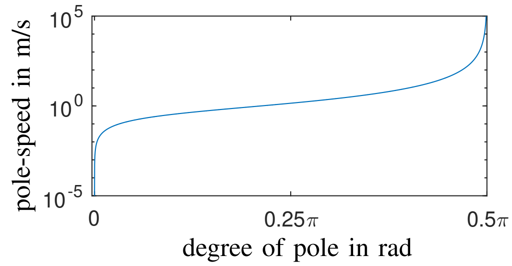

Fig. 3. The speed of a rod needed at a certain angle for a rotation speed of 1 rad/s for a sphere of 1 m radius.

one extension speed to maintain a constant ω. For the slowest possible rotation speed we use the biggest possible θ which is still extending, i.e. α. This holds for all the following experiments.

b) Leverage Approach:

For the second approach of creating torque for the sphere by leverage, extending the poles between π rad and 2π rad leads to weight leverage, creating a clockwise rotation that leads to translation. As this relies entirely on the mass of the poles, for poles that are too lightweight, the static friction is too large to generate movement via the leverage torque. Nevertheless, its application as support for the pushing approach is still feasible. For this approach, we need to avoid collision of the pole with the ground, as this stops the rotation and may even lead to reverse rotation. The change of the maximum possible length of a pole decreases from 1.5π rad to 2π rad rapidly. Therefore, there exists an angle γ, at which the maximum retraction speed of a rod matches the needed retraction speed. At this angle, a pole is capable of retracting itself without colliding with the ground. Let $\dot{l}_{\text{max}}$ be the maximum speed of a pole, ω the rotation speed of the sphere and r_m the radius of the sphere. For sake of readability we define

$$k := \frac{-\dot{l}_{\text{max}}}{r \cdot \omega}\,. \tag{5}$$

It then follows:

$$-\dot{l}_{\text{max}} = r \cdot \omega \cdot \tan(\gamma)\sec(\gamma)$$

$$\Leftrightarrow \gamma = \pi + 2\arctan\left(\frac{1}{2}\sqrt{\frac{1}{k^2} + 4} + \frac{\sqrt{\frac{1}{k^2} - \frac{4}{k\sqrt{1/k^2+4}} - \frac{1}{k^3\sqrt{1/k^2+4s}}}}{\sqrt{2}} - \frac{1}{2k}\right)\,. \tag{6}$$

Due to the finite length of a pole, there exists an angle ζ_{touch}, at which the fully extended pole touches the ground. Let l_{max} be the maximum length of a pole, r_s the radius of the side disc where the poles are mounted and r_m the radius of the sphere, then this touchpoint angle is given by

$$\zeta_{\text{touch}} = \arccos\left(\frac{l_{\text{max}} + r_s}{r_m}\right)\,. \tag{7}$$

If γ is less or equal to this angle, accurately timed retraction of the pole is always ensured. This means the retraction of

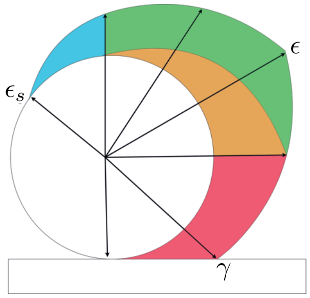

Fig. 4. Visualization of ε_s, ε, γ and the relevant area representing the integration of the overall torque. Blue: Area where torque is generated in the opposite direction than intended. Orange: Area where torque is generated if the extensions start at π rad. Full extension is not reached due to the short extension time. Green: Area where torque is generated if the extension starts at ε_s, in addition to the orange area. Red: Area that both approaches cover.

the pole is managed, that it always just avoids the collision at the next moment by adapting the retraction velocity. For smaller γ, we need to retract a pole at full speed before γ in a way that at γ, the rod has just the maximum possible length at that moment. Therefore, there exists an angle ε, at which we need to start retraction at full speed in order to reach γ with the right length. As a consequence of the maximum extension at ε, there exists an angle ε_s, at which the extension needs to start to reach the maximum extension at ε. If this ε_s lies on the other side of the intended rotation, i.e., ε_s less than π rad, in between ε_s and π rad, the rod produces torque in the wrong direction. An alternative strategy generates only torque in the desired direction by starting the extension at π rad, continuing until 1.5π rad to a certain length and then retracting at full speed until reaching γ. Figure 4 shows these two approaches and the areas in which torque is generated.

This raises the question whether the ε approach is beneficial. For the evaluation, if the assumption of an ε_s is valid, we anticipate that a single mass point at distance $r(\zeta)$ introduces a torque

$$\tau = r(\zeta) \cdot (-\sin(\zeta)) \cdot q\,, \tag{8}$$

where q is a constant depending on physical specifications of the robot and poles. Thus, we integrate the torque generated by one pole over the process of one rotation. We integrate τ from Equation (8), leading to

$$\tau = \int_0^{2\pi} r(\zeta) \cdot ((-\sin(\zeta))) \cdot q\, d\zeta\,. \tag{9}$$

If we start extending at π, hence ignoring the calculated values for the extension ε_s and retraction ε, this leads to

$$\begin{aligned}
\tau_\pi &= \int_\pi^{2\pi} r(\zeta) \cdot (-\sin(\zeta)) \cdot q\, d\zeta & (10)\\
&= \int_\pi^{1.5\pi} r(\zeta) \cdot (-\sin(\zeta)) \cdot q\, d\zeta \\
&\quad + \int_{1.5\pi}^{\gamma} \dot{l}_{\max} \cdot (\pi - \zeta) \cdot (-\sin(\zeta)) \cdot q\, d\zeta \\
&\quad + \int_{\gamma}^{2\pi} (\frac{r}{cos(\zeta)} - r) \cdot (-\sin(\zeta)) \cdot q\, d\zeta & (11)
\end{aligned}$$

Here, we make one simplification – assuming that the retraction starts at 1.5π rad. This will always lead to less torque than in reality as the decreased speed of the retraction from γ will result in an overall less extension in the first part. Therefore, this is a lower bound. If we take ε_s as the starting point, also using the 1.5π assumption, this leads to

$$\begin{aligned}
\tau_{\varepsilon_s} &= \int_{\varepsilon_s}^{\varepsilon} r(\zeta) \cdot ((-\sin(\zeta))) \cdot q\, d\zeta \\
&\quad + \int_{\varepsilon}^{1.5\pi} r(\zeta) \cdot (-\sin(\zeta)) \cdot q\, d\zeta \\
&\quad + \int_{1.5\pi}^{\gamma} r(\zeta) \cdot (-\sin(\zeta)) \cdot q\, d\zeta \\
&\quad + \int_{\gamma}^{2\pi} \dot{l}_{\max}(\zeta - \varepsilon) \cdot (-\sin(\zeta)) \cdot q\, d\zeta\,. & (12)
\end{aligned}$$

Here, the angles at which torque is generated are divided from ε_s to ε where they extend, from ε to γ where they retract at full speed, and γ to 2π where retraction is at adjusted speed. The range between ε to γ is again divided into ε to 1.5π and 1.5π to γ, as this is helpful for further evaluation since this is the same limit for integration as used in the calculation of τ_π. Now we substitute the corresponding calculations for $r(\zeta)$ for each integration block:

$$\begin{aligned}
\tau_{\varepsilon_s} &= \int_{\varepsilon_s}^{\varepsilon} \dot{l}_{\max}(\zeta - \varepsilon_s) \cdot ((-\sin(\zeta))) \cdot q\, d\zeta \\
&\quad + \int_{\varepsilon}^{1.5\pi} ((\varepsilon - \varepsilon_s)\dot{l}_{\max} - \dot{l}_{\max} \cdot (\zeta - \varepsilon))) \\
&\quad \cdot(-\sin(\zeta)) \cdot q\, d\zeta \\
&\quad + \int_{1.5\pi}^{\gamma} \dot{l}_{\max} \cdot (\pi - \zeta) \cdot (-\sin(\zeta)) \cdot q\, d\zeta \\
&\quad + \int_{\gamma}^{2\pi} (\frac{r}{cos(\zeta)} - r) \cdot (-\sin(\zeta)) \cdot q\, d\zeta\,. & (13)
\end{aligned}$$

Presume that Equation (13) is less than or equal to Equation (11), i.e. $\tau_\pi \leq \tau_{\varepsilon_s}$, it follows

$$\begin{aligned}
&\int_{\pi}^{1.5\pi} \dot{l}_{\max} \cdot (\zeta - \pi) \cdot (-\sin(\zeta)) \cdot q\, d\zeta \\
&+ \int_{1.5\pi}^{\gamma} \dot{l}_{\max} \cdot (\pi - \zeta) \cdot (-\sin(\zeta)) \cdot q\, d\zeta \\
&+ \int_{\gamma}^{2\pi} (\frac{r}{\cos(\zeta)} - r) \cdot (-\sin(\zeta)) \cdot q\, d\zeta \\
&\leq \int_{\varepsilon_s}^{\varepsilon} \dot{l}_{\max}(\zeta - \varepsilon_s) \cdot ((-\sin(\zeta))) \cdot q\, d\zeta \\
&+ \int_{\varepsilon}^{1.5\pi} ((\varepsilon - \varepsilon_s)\dot{l}_{\max} - \dot{l}_{\max} \cdot (\zeta - \varepsilon))) \\
&\quad \cdot(-\sin(\zeta)) \cdot q\, d\zeta \\
&+ \int_{1.5\pi}^{\gamma} \dot{l}_{\max} \cdot (\pi - \zeta) \cdot (-\sin(\zeta)) \cdot q\, d\zeta \\
&+ \int_{\gamma}^{2\pi} (\frac{r}{\cos(\zeta)} - r) \cdot (-\sin(\zeta)) \cdot q\, d\zeta\,. & (14)
\end{aligned}$$

And, maintaining the assumption that there is no torque for angles larger than 1.5π rad, this results in

$$
\begin{aligned}
&\int_{\pi}^{1.5\pi} \dot{l}_{\max} \cdot (\zeta-\pi) \cdot (-\sin(\zeta)) \cdot q \, d\zeta \\
\leq\ & \int_{\varepsilon_s}^{\varepsilon} \dot{l}_{\max}(\zeta-\varepsilon_s) \cdot ((-\sin(\zeta))) \cdot q \, d\zeta \\
&+ \int_{\varepsilon}^{1.5\pi} ((\varepsilon-\varepsilon_s)\dot{l}_{\max} - \dot{l}_{\max} \cdot (\zeta-\varepsilon))) \\
&\quad \cdot (-\sin(\zeta)) \cdot q \, d\zeta \, . \qquad (15)
\end{aligned}
$$

Solving this numerically gives a valid range of $1.11\pi < \varepsilon \leq 1.5\pi$. Hence, the previously stated hypothesis is false. It is not always beneficial to use an ε_s start rather than the π rad start, whereas it is the case if ε is greater than 1.11π rad. Evaluating the right side of Equation (15) shows a maximum at $\varepsilon = 1.31\pi$ rad. Previously, we simplified the starting point of the retraction as 1.5π rad, which we need to reevaluate as the hypothesis was not confirmed. However, with the new knowledge of a maximum, we can cut short the long and complicated integration of γ by specifying the upper limit for integration as $1.5\pi - \frac{\gamma}{2}$. Starting retraction at $1.5\pi - \frac{\gamma}{2}$ leads to full retraction at γ. Therefore, this is the absolute worst case, but this time, for the ε_s approach, as angle of the upper limit for integration on the right side decreases. Therefore, the positive torque also decreases. At the same time, the undesired torque on the left side stays the same. Repeating all the previous steps from Equation (11) onward, yields

$$
\begin{aligned}
&\int_{\pi}^{1.5\pi-\frac{\gamma}{2}} \dot{l}_{\max} \cdot (\zeta-\pi) \cdot (-\sin(\zeta)) \cdot q \, d\zeta \\
\leq\ & \int_{\varepsilon_s}^{\varepsilon} \dot{l}_{\max}(\zeta-\varepsilon_s) \cdot ((-\sin(\zeta))) \cdot q \, d\zeta \\
&+ \int_{\varepsilon}^{1.5\pi-\frac{\gamma}{2}} ((\varepsilon-\varepsilon_s)\dot{l}_{\max} - \dot{l}_{\max} \cdot (\zeta-\varepsilon))) \\
&\quad \cdot (-\sin(\zeta)) \cdot q \, d\zeta \, . \qquad (16)
\end{aligned}
$$

Inserting the previously found $\varepsilon = 1.31\pi$ rad and numerically solving for γ leads to no solution within the logical range of 1.5π rad to 2π rad. Therefore, we found a value for $\pi < \varepsilon \leq 1.5\pi$ rad, which will always be beneficial in comparison to a start of the extension at π, for any γ. This leads to an alternative definition of ε as it was initially defined as the starting angle for the retraction for reaching γ in time. With this evaluation, we showed that it is beneficial to always have the maximum extension at a certain ε. Note that the said maximum extension does not necessarily refer to $l_{\max}$. It describes that if a full extension is not possible with a start at π, the extension should start at ε_s; therefore, it is not guaranteed that $l_{\max}$ is reached at ε, as it cannot be retracted in time before reaching γ. This leads to the conclusion that we cannot calculate ε_s by just factoring in the time needed for full extension. In fact, we need to calculate an extension of the poles that can be retracted between ε and 2π rad. From ε to γ, the retraction happens with full speed and from γ to 2π rad with a reduced speed. There certainly exists a solution for ε_s. However, in our opinion, this goes into directions where the benefit for practical implementation does not hold up to the required computational power and the needed precision of all actions. For the prototype introduced later, this is not even possible as there is no feedback on the pole length. Therefore, we conclude that if the combination of pole length, the retraction speed of the pole, and the desired rotation speed are in a relevant range, and the feedback on the exact extension length is given, we implement the adapted ε mechanism. At each calculation cycle, we determine the new γ; on the basis of this, we find the maximum of Equation (16), giving us the optimal ε, which is then used to calculate the needed ε_s. In the further evaluation, we refer to this step just as "calculating γ, ε, and ε_s". It is incumbent on the actual robot and the requirement if certain described adaptions are made. Therefore, we also ignore these values if the retraction speed is always fast enough to retract in time ($\gamma = 1.5\pi$ rad). For the vast majority of all implementations, this will be sufficient and reduces complexity to a minimum. Algorithm 1 shows the pseudo-code for a push and leverage algorithm, taking all these parameters into account.

Algorithm 1: Leverage and Push Movement Algorithm with detailed boundaries and limitations.

```
repeat
    calculate γ, ε and ε_s
    foreach pole x do
        predict ζ_x with measured ω & commanded c_ω
        if β ≤ ζ_x ≤ α then
            extend pole
        else if retraction speed > maximum retraction
          speed needed then
            if ζ_x > π and no contact to ground then
                extend pole
            else
                retract pole (ground avoidance mode)
            end
        else if ζ_x > γ then
            retract pole (ground avoidance mode)
        else if (ζ_x > ε_s  or  ζ_x > π)  and  ζ_x > α
          then
            extend pole
        else
            retract pole
        end
    end
end
```

c) Balancing:

Balancing ensures a constant angle to the sides while rolling forward or remaining stationary. As this is a conservation of a certain condition, closed-loop control is adopted for this problem, rather than an open-loop algorithm like for the locomotion. As this is a vast field and, like most closed-loop controlling systems, very dependent on parameter tuning, we will focus on the problem taking the limitations of our used prototype into account. This means mono-speed extension and no feedback on the actual extension. The three controllable states of our used poles are “Extend”, “Retract”, and “Hold”. For poles with variable speed the speed itself can be taken as system input, which gives a huge variety of controllers that are theoretically able to solve the problem. But for mono-speed poles there are no other options than using these three states. The control itself is relatively simple. This comes with simplifications, such as omitting an anti-windup system, as there is no unlimitedly increasing or decreasing value, just the three states with no further changeable value. The three-point controller is realized by accepting a specific range of roll error, in our case ± 3 degree, and with the transgression of this value extending the poles on the side the robot is falling towards and retracting on the other side. While in the accepted range, the poles are just on “Hold” maintaining their length. In theory, there exists an optimal lengthl_{balance} for the pole if the robot is on flat ground. Let r_m be the radius of the middle disc, i.e. the radius of the sphere and r_s the radius of the disc the poles are mounted on, then

$$l_{\text{balance}} = \frac{r_m}{\cos \zeta} - r_s \,. \tag{17}$$

Of course, this yields for $0.5\pi\text{rad} < \zeta < 1.5\pi$ rad and assumes the minimum extension as $r_m - r_s$. We use the knowledge of this length to our advantage, even if there is no possibility to control the length of a pole directly, just the speed. If after the start the robot tilts to one side and this is compensated by the rods on the other side and by the momentum the robot falls to the other side, the poles are still completely retracted on this side. If the speed of the poles is too slow, the robot will fall more on the other side until the rods on that side reach the ground at all. Accordingly, the previously mentioned optimum length or at least a minimum length should be aimed for. With feedback of the length of the rods, the optimum length or at least a minimum length can be aimed for at any time. Without feedback, only the integration with the assumed speed and time remains. This length becomes more inaccurate with each action. Since a complete retraction or extension to know the length again for sure is not an option when balancing, only an initial extension to the desired length remains. For our purposes, this turns out to be enough to select a stable roll-angle.

Experiments and Results

For a spherical robot the choice of which rods to use and when to extend and retract them for locomotion and for balancing overshadow each other. Therefore, the initial evaluation of different movement methods is done using a cylindrical design. The initial prototype consists of three similar discs, connected by props. Later, the middle disc is enlarged and a spherical shell is added to surround the structure. Both prototypes are shown in Figure 5. The two side-discs each hold eight telescopic-extendable rods. Both-disc structures with electronics weigh 20.7 kg, and with the spherical prototype the shell adds 17.15 kg to an overall 37.85 kg. The poles have a force of 12.25 N. (corresponding to pushing 1.25 kg on earth). The side discs have a

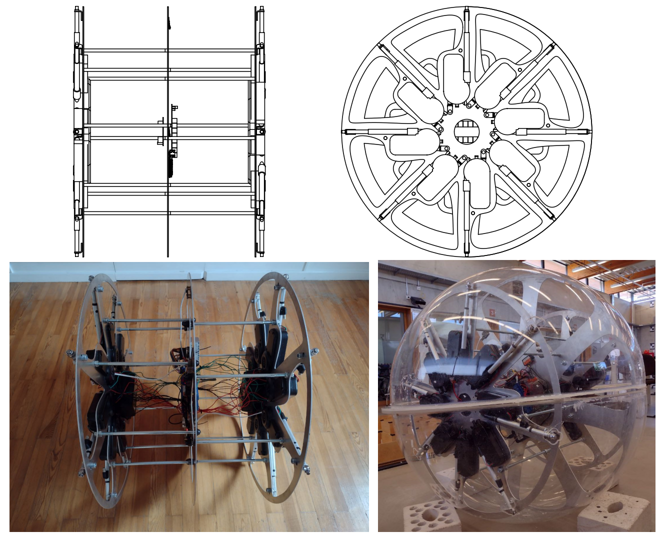

Fig. 5. Above, and below left: first cylindrical prototype. Below right: successor prototype with the central disc enlarged and the outer shell.

diameter of 80 cm, which therefore is also the diameter of the cylindrical prototype. The spherical prototype has an overall diameter of 100 cm. For the pose estimation, we use three Inertial Measurement Units (IMU). The spherical shape allows for improving the pose estimation with the knowledge of the behavior of such robots regarding the connection between rotation and translation. [5] proposes such a pose-estimation algorithm adapted for spherical robots, which is used for our prototypes. The fundamental approaches of rotation by pushing, leverage, and the combination of both have been evaluated on the cylindrical prototype. For pushing the grip is crucial and leads with the same parameters to very different results. This is shown for three different surfaces in Figure 6. Rotation is initialized using $\alpha = 57°$ and $\beta = 2°$ and the resulting rotation speed is measured using the IMUs with the aforementioned algorithm. The shown rotation speed is the unfiltered raw data of that algorithm. The smoothest behavior and the fastest rotation is achieved on the gravelly ground whereas on the flat sealed surface the sphere decelerates again after each push reducing the maximum speed to half compared to the gravelly ground.

This is due to a slip each pole experiences when it is in contact with the ground. In other words, the pole bends as its tip slips over the ground until the bend is big enough so that further bending requires more force than initiating rotation. The pole at angles near α extends but bends as the tip slips over the flat surface. When extending the next rod near β, the pole bends back, leading to the oscillation and taking away the better force transition from the rod with small angles, leading to an overall slower rotation speed. As expected, for smaller α this behavior is reduced but not completely prevented. Having rather big obstacles (stones etc.) or having just ground with increased grip (outdoor, rough asphalt, etc.) does not allow, or at least minimizes, such behavior. At some point, the pole tip gets canted, even if only minimal. As the extension speed of the mono-speed poles cannot be varied based on the angles, the induced acceleration when touching the ground differs depending on the angle, leading to the

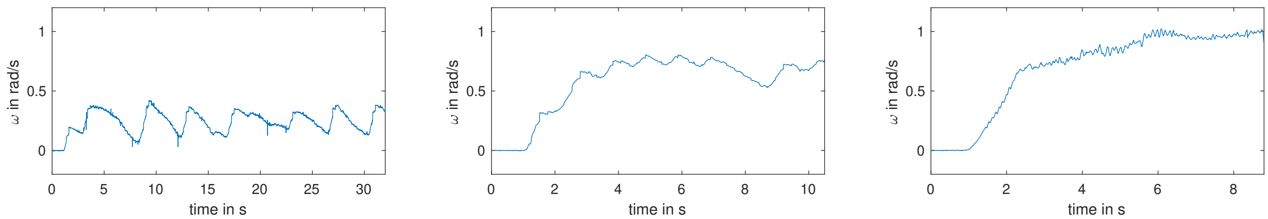

Fig. 6. Rotation speed results of the cylindrical prototype on different surfaces with the rotation by pushing approach. Left: Flat, sealed ground. Middle: Wooden floorboard. Right: Gravelly ground. For all experiments α was set to 57 degree and β to 2 degree.

oscillations seen in all the plots.

This raises the question about the behavior on the moon surface, which also has many sandy and dusty surfaces. On soft and sandy ground our prototype fails to initiate rotation. This is due to the increased rolling resistance and the limited strength of the actuators. But the poles did reach a certain point (several centimeters) where they did not sink any further. Therefore we assume that with strong enough actuators, a rotation is still possible and might even lead to a smoother rotation, due to the damped system. This question and the eventual enlarging of the end of the rod for more surface area will be investigated with an improved prototype in future work.

For the solid surfaces, we tested different angles of α and β for the pushing approach. Thereby we verified, that a too low β has a negative effect on the locomotion. Figure 7 shows the result of two locomotion test-runs with both an overall $\alpha\beta$ difference of $45\,^\circ$ but one starting with a β of $0\,^\circ$ and the other with $2\,^\circ$. The $0\,^\circ$ leads clearly to a more oscillating behavior. This is caused by the rods starting to extend perpendicular to the ground. Force is build up force as the rod fails to physically extend and lacks enough force to push the robot directly upwards. This build up force unloads once ζ increases a little bit, inducing huge acceleration which leads to an immediate failure of the pole to touch the ground within the $alpha$ range due to the limited extension speed. This ultimately results in the seen oscillating behavior, whereas with the higher β this force into the ground is never build up but directly transformed into rotation.

Further experiments are shown in the first supplementary video. To summarize the outcomes: The basic balancing algorithm works for the unstable disc setup and for the full spherical setup. Here, the pole strength is enough to provide controllability of the roll angle. The roll angle remains stable without oscillations. Based on a theoretical model the maximum inclination the prototype can traverse is computed as $4.1\,^\circ$ for the pushing approach, $0.92\,^\circ$ for leverage. For push and leverage together the leverage part is concluded to be neglectable, Slope experiments confirm this assumption with the maximum possible inclination in the same order of magnitude (Push and Leverage achieved $3.7\,^\circ$, Push Only $3.6\,^\circ$ and Leverage only $1.3\,^\circ$ (the experiment is shown in Figure 8). For reference, the same calculations with the gravitational force on the moon lead to $36.8\,^\circ$ possible inclination, assuming perfect grip. For the pole mechanism in general, there is no real general slope limit, as linear telescopic poles weighing less than 0.5 kg easily bring up 300 N. Inserting such huge power leads to maximum slopes of 0.5π rad, which means these poles are capable of pushing the robot straight up, at least in a purely mathematical sense. Evaluating the locomotion for the full spherical setup reveals that the leverage-only approach fails to move the robot as the spherical shell increases the weight significantly. With the push-only approach, the sphere pushes itself into a stall position. When adding leverage, the prototype overcomes the stall position but fails to initiate a stable forward motion, falling into a non-compensatable roll, which needs to be reset manually.

Conclusions and Future Work

Rod-driven locomotion is a promising approach for spherical robots in rough terrains. The paper has investigated the basic principles of locomotion using extendable rods.

Needless to say, a lot of work remains to be done. In further research we will investigate a more robust version of the prototype, especially in terms of more powerful actuators. This will allow the evaluation of uniform rotational

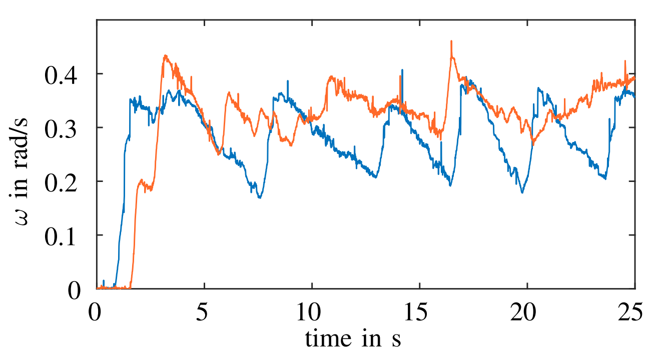

Fig. 7. Rotation speed of the sphere with the push only approach. Blue: α= $45\,^\circ$, β=$0\,^\circ$. Orange: α= $47\,^\circ$, β=$2\,^\circ$. Despite both cases extending over an area of $45\,^\circ$, the too low β of the first case leads to oscillations.

Fig. 8. Slope experiments. The robot rolls up a ramp with increasing slope. The slope is then measured with a water level at the place where the robot stops. Here the Push and Leverage approach is tested.

speeds that cannot be achieved with single-speed actuators. In addition, this type of locomotion theoretically gives robots the ability to overcome vertical obstacles. Sufficiently powerful actuators are required to demonstrate this. This new ability for climbing also required a controller, which decides whether to use the normal locomotion algorithm or change to a special climbing mode. Also, we will investigate an improved algorithm for combination of balancing and locomotion and the inclusion of sensor-data for a better decision-making of the rod-extensions due to information about the terrain.

References

[1] Angelo Pio Rossi, et al. DAEDALUS-Descent and Exploration in Deep Autonomy of Lava Underground Structures: Open Space Innovation Platform (OSIP) Lunar Caves-System Study. 2021.

[2] David S McKay, et al. The lunar regolith. *Lunar sourcebook*, 1991.

[3] John V Gies. The effect of the lunar surface environment upon machinery. In *Engineering, Construction, and Operations in Space V*, 1996.

[4] Vincent A Crossley. A literature review on the design of spherical rolling robots. , 2006.

[5] Jasper Zevering, Anton Bredenbeck, Fabian Arzberger, Dorit Borrmann, and Andreas Nüchter. Imu-based pose-estimation for spherical robots with limited resources. In *IEEE Conference on Multisensor Fusion and Integration for Intelligent Systems (MFI)*, 2021.

[6] Richard Chase and Abhilash Pandya. A review of active mechanical driving principles of spherical robots. , 2012.

[7] Atsushi Koshiyama and Kazuo Yamafuji. Design and control of an all-direction steering type mobile robot. *The International journal of robotics research*, 1993.

[8] Daliang Liu, Hanxv Sun, Qingxuan Jia, and Liangqing Wang. Motion control of a spherical mobile robot by feedback linearization. In *2008 7th World Congress on Intelligent Control and Automation*, 2008.

[9] H Vahid Alizadeh and Mohammad J Mahjoob. Quadratic damping model for a spherical mobile robot moving on the free surface of the water. In *2011 IEEE (ROSE)*, 2011.

[10] Deepak Pokhrel, Nutan Rajm Luitel, Sukanta Das, and Dip Narayan Ray. Design and development of a spherical robot (spherobot). in *iNaCoMM2013*, 2013.

[11] Saeed Moazami, Srinivas Palanki, and Hassan Zargarzadeh. Kinematics of norma, a spherical robot, rolling over 3d terrains. *American Control Conference (ACC)*, IEEE, 2019.

[12] Maotao Yang, et al. Design and analysis of a spherical robot with two degrees of freedom swing. In *Chinese Control And Decision Conference (CCDC)*, IEEE, 2020.

[13] Saber Mahboubi, Mir Masoud Seyyed Fakhrabadi, and Ahmad Ghanbari. Design and implementation of a novel spherical mobile robot. *Journal of Intelligent & Robotic Systems*, 2013.

[14] Joong-Cheol Yoon, Sung-Su Ahn, and Yun-Jung Lee. Spherical robot with new type of two-pendulum driving mechanism. In *IEEE - 15th INES*, 2011.

[15] Viktor Kaznov and Mattias Seeman. Outdoor navigation with a spherical amphibious robot. In *IEEE/RSJ - IROS*, 2010.

[16] Puyan Mojabi, et al. Introducing august: a novel strategy for an omnidirectional spherical rolling robot. In *IEEE - ICRA*, 2002.

[17] Ranjan Mukherjee, Mark A Minor, and Jay T Pukrushpan. Simple motion planning strategies for spherobot: a spherical mobile robot. In *IEEE - 38th CDC*, 1999.

[18] James Lux. Alternative way of shifting mass to move a spherical robot. *NTRS: NASA Technical Reports*, 2005.

[19] Wei Zhao, Han Xu Sun, Qing Xuan Jia, Yan Heng Zhang, and Tao Yu. Mechanical analysis of the jumping motion of a spherical robot. In *Advanced Materials Research*, 2012.

[20] Tomi Ylikorpi and Jussi Suomela. Ball-shaped robots. In *Climbing & Walking Robots, Towards New Applications*, 2007.

[21] Aarne Halme, Torsten Schonberg, and Yan Wang. Motion control of a spherical mobile robot. In *IEEE - AMC - MIE*, 1996.

[22] J Alves and J Dias. Design and control of a spherical mobile robot. *Proceedings of the Institution of Mechanical Engineers*, 2003.

[23] Qiang Zhan, Yao Cai, and Caixia Yan. Design, analysis and experiments of an omni-directional spherical robot. In *IEEE - ICRA*, 2011.

[24] Wei-Hsi Chen, Ching-Pei Chen, Jia-Shiuan Tsai, Jackie Yang, and Pei-Chun Lin. Design and implementation of a ball-driven omnidirectional spherical robot. *Mechanism and Machine Theory*, 2013.

[25] Harry Duong Nguyen, Gim Soh, Shaohui Foong, and Kristin Wood. De-coupled dynamics control of a spherical rolling robot for waypoint navigation. In *2017 IEEE - CIS and IEEE - RAM*, 2017.

[26] Yury L Karavaev and Alexander A Kilin. The dynamics and control of a spherical robot with an internal omniwheel platform. *Regular and Chaotic Dynamics*, 2015.

[27] Yu L Karavaev and Aleksandr Aleksandrovich Kilin. Nonholonomic dynamics and control of a spherical robot with an internal omniwheel platform: Theory and experiments. *Proceedings of the Steklov Institute of Mathematics*, 2016.

[28] Giulio Reina, Mario Foglia, Annalisa Milella, and Angelo Gentile. Rough-terrain traversability for a cylindrical shaped mobile robot. In *IEEE - ICM*, 2004.

[29] Zhan Qiang, Liu Zengbo, and Cai Yao. A back-stepping based trajectory tracking controller for a non-chained nonholonomic spherical robot. *Chinese Journal of Aeronautics*, 2008.

[30] Shourov Bhattacharya and Sunil K Agrawal. Spherical rolling robot: A design and motion planning studies. *IEEE Transactions on Robotics and Automation*, 2000.

[31] Jasper Zevering, Anton Bredenbeck, Fabian Arzberger, Dorit Borrmann, and Andreas Nüchter. Luna-a laser-mapping unidirectional navigation actuator. In *IEEE - ISER*, 2020.

[32] Brian Chemel, Edward Mutschler, and Hagen Schempf. Cyclops: Miniature robotic reconnaissance system. In *IEEE - ICRA*, 1999.

[33] Jia Qingxuan, Zheng Yili, Sun Hanxu, Cao Hongyu, and Li Hongyi. Motion control of a novel spherical robot equipped with a flywheel. In *IEEE - ICIA*, 2009.

[34] Rhodri Armour, Keith Paskins, Adrian Bowyer, Julian Vincent, and William Megill. Jumping robots: a biomimetic solution to locomotion across rough terrain. *Bioinspiration & biomimetics*, 2007.

[35] Yuuta Sugiyama and Shinichi Hirai. Crawling and jumping of deformable soft robot. In *2004 IEEE/RSJ - IROS*, 2004.

[36] Kyunam Kim, et al. Hopping and rolling locomotion with spherical tensegrity robots. In *2016 IEEE/RSJ - IROS)*, 2016.

[37] Lee-Huang Chen, et al. Soft spherical tensegrity robot design using rod-centered actuation and control. *Journal of Mechanisms and Robotics*, 2017.

[38] Adrian K Agogino, Vytas SunSpiral, and David Atkinson. Super ball bot-structures for planetary landing and exploration. *NASA Innovative Advanced Concepts (NIAC) Program*, 2018.

[39] Keith W Wait, Philip J Jackson, and Lanny S Smoot. Self locomotion of a spherical rolling robot using a novel deformable pneumatic method. In *IEEE - ICRA*, 2010.

[40] Young-Min Kim, Sung-Su Ahn, and Y Lee. Kisbot: new spherical robot with arms. In *WSEAS - 10th ICRCMT*, 2010.

[41] Ingo Rechenberg, et al. Bionicwheelbot - walk and roll like a flic-flac spider. `https://www.festo.com/net/SupportPortal/Files/492805/Festo_BionicWheelBot_en.pdf`, 2018. Accessed: 22-07-2021.

[42] Ralf Simon King. BiLBIQ: A biologically inspired robot with walking and rolling locomotion, 2012.

[43] Jorge Ocampo-Jimenez, Angelica Muñoz-Meléndez, and Gustavo Gómez. Enhanced locomotion of a spherical robot based on the sea-urchin characteristics. In *Biomimetic and Biohybrid Systems*, pages 238–248, Cham, 07 2014. Springer International Publishing.

Supplementary Materials

A video demonstrating and showing further experiments of the presented approach is given under the following URL: `https://youtu.be/NyrgArI2zKg`

A video of the DAEDALUS study is available under the following URL:
`https://youtu.be/69CrH9vsTTU`